Density Functional Theory Characterization of the Structure and Gas-Phase, Mid-Infrared Absorption Spectrum of 2-Azido–N,N-Dimethylethanamine (DMAZ)

by Michael J. McQuaid, Kevin L. McNesby, Betsy M. Rice, and Cary F. Chabalowski

ARL-TR-2770   July 2002

20020709 133

Army Research Laboratory
Aberdeen Proving Ground, MD 21005-5066

Density Functional Theory Characterization of the Structure and Gas-Phase, Mid-Infrared Absorption Spectrum of 2-Azido–N,N-Dimethylethanamine (DMAZ)

Michael J. McQuaid, Kevin L. McNesby, Betsy M. Rice, and Cary F. Chabalowski
Weapons and Materials Research Directorate, ARL

Abstract

Non-local density functional theory utilizing the B3LYP exchange-correlation functionals with a 6-311++G(d,p) basis set was employed to characterize the geometric parameters and normal modes of 12 equilibrium conformations of 2-azido–N,N-dimethylethanamine. Also known as DMAZ, an experimentally acquired mid-infrared absorption spectrum of this fuel's vapor is analyzed based on the computational results. The analysis indicates that the relative populations of DMAZ conformers in a room-temperature sample do not deviate significantly from expectations based on a Boltzmann distribution calculated from their theoretically determined zero-point corrected energies. The most abundant conformer is found to have the central nitrogen atom of the azido group aligned over the amine lone pair electrons. Since this configuration is likely to inhibit proton transfer to the amine site, it may play an influential role in DMAZ's performance as a hypergol.

Acknowledgments

INTENTIONALLY LEFT BLANK.

Contents

INTENTIONALLY LEFT BLANK.

List of Figures

List of Tables

INTENTIONALLY LEFT BLANK.

1. Introduction

Providing an extremely reliable basis on which to design intermittent and/or variable thrust propulsion systems, hypergolic liquid (or gel) fuel-oxidizer combinations—i.e., those that react spontaneously upon mixing—are employed throughout the U.S. Department of Defense (DOD) and the National Aeronautics and Space Administration (NASA) for aviation and missile applications. One of the drawbacks to "standard" hypergolic fuel-oxidizer combinations, however, is that the fuels are derived from hydrazine, monomethylhydrazine (MMH), and/or unsymmetrical dimethylhydrazine (UDMH)—all of which are acutely toxic and suspected carcinogens. As a result, their use requires burdensome and costly handling procedures.

Searching for alternatives to hydrazine-based fuels, the Army is investigating the use of secondary and tertiary amine azides in various propulsion applications, a formulation within this class of compounds receiving considerable attention being 2-azido-N,N-dimethylethanamine [$(CH_3)_2NCH_2CH_2N_3$]. Also referred to as DMAZ, this fuel is found to perform competitively with Aerozine 50 (a 50/50 mixture of hydrazine and UDMH) in inhibited red fuming nitric acid (IRFNA) oxidized experimental systems. DMAZ-IRFNA systems do not, however, meet "ignition delay" standards set by MMH-IRFNA systems. Longer ignition delays—i.e., the time that elapses from the moment that the fuel and oxidizer are mixed until a combustion flame or significant pressure increases is observed— require the design of larger combustion chambers to avoid "hard starts." Since larger combustion chambers penalize rocket performance, DMAZ's ignition delays may negatively impact the Army's ability to field it.

Hoping to reduce ignition delays by identifying rate-limiting mechanisms within hypergolic ignition processes (and means to bypass them), the reaction chemistry associated with such processes is being studied. In the case of DMAZ-IRFNA systems, testing indicates that proton transfer from nitric acid to the amine nitrogen is an important step. To evaluate this finding and its potential utility as a basis for obtaining hydrazine-based fuel performance with hydrazine alternatives, computational quantum chemistry is being employed to characterize fuel-nitric acid proton transfer reaction pathways. If ignition delays prove to correlate with the energetics associated with such pathways, it may be possible to specify conditions that enhance DMAZ's performance or design and computationally screen new fuels based on what is learned.

This report summarizes the completion of the first phase of a study of DMAZ-nitric acid reactions, namely, characterization of DMAZ equilibrium conformers.

Utilizing non-local density functional theory (DFT), 12 equilibrium structures were identified, and their geometries and normal mode characteristics are presented here. In addition, the results of the computational study were corroborated by comparing them to a gas-phase, mid-infrared (IR) DMAZ (vibrational) absorption spectrum acquired experimentally. Based on results obtained with a non-linear, least-squares fitting routine employed to facilitate the comparison, spectral assignments are proposed, and the relative energies of the structures are evaluated.

2. Computational Methods

All computations were performed with the Gaussian 98 (G98) suite of quantum chemistry codes [1]. DFT utilizing the B3LYP exchange-correlation functionals [2-4] and a 6-31+G(d,p) atomic orbital basis set [5-10] was employed in initial calculations to identify DMAZ equilibrium conformations. Diffuse functions [11] were included in anticipation of the need to characterize proton transfer leading to nitrate salt (ion pair) formation in the follow-on to this study. "Very tight" energy gradient convergence criteria (as defined by G98) were invoked during the geometry optimization procedure in an unsuccessful attempt to remedy large (>20 cm⁻¹) rotational/translational mode eigenvalues appearing in the normal mode analysis of some structures obtained with the default criteria. A larger basis set [6-311++G(d,p)] [12, 13] with the G98-defined "ultrafine" grid was later employed to characterize the conformers identified in the initial survey. The 6-311++G(d,p) basis set was chosen based on its use in ammonia-nitric acid-water reaction studies published by Tao and coworkers [14, 15], their results expected to provide benchmarks for planned hypergol-nitric acid reaction studies. The use of the ultrafine grid resolved the issue with the size of rotational/translational mode eigenvalues appearing in the initial survey, an issue not rectified by the use of a larger basis set [6-311+G(2d,2p)] alone.

The search for transition state structures connecting local minimum structures was conducted through the use of the Synchronous Transit Guided Quasi-Newton (STQN) method available within G98 [16, 17]. For selected representative transformations, verification that the transition state found by the method connected the two local minimum structures employed to start the search was obtained via intrinsic reaction coordinate (IRC) walks [18, 19]. All other transition state-local minima connections were established or verified by comparing the transition state's geometry with local minimum geometries and inspecting the motion associated with the transition state's imaginary eigenmode.

3. Experimental Methods

To corroborate the results of the computational study, mid-IR absorption spectra for gas-phase DMAZ were acquired experimentally. A DMAZ sample was provided by the 3M Corp. and used without further purification. The absorption spectra were measured using a Fourier transform infrared spectrometer (Bomem Inc., model DA-8) interfaced to an evacuable variable-pathlength cell (Foxboro Analytical) equipped with silver bromide windows. With the cell pathlength set to 225 cm, measurements were made on samples obtained by allowing vapor above room temperature DMAZ liquid to expand into the evacuated cell; the final total pressure within the cell reaching approximately 2.5 Torr. Modulated radiation from the spectrometer was detected using a liquid nitrogen-cooled HgCdTe detector, 256 scans at 0.1-cm^{-1} resolution being co-added to yield the spectrum presented in this report.

4. Theoretical Results

Figure 1 shows all of the equilibrium DMAZ structures identified through this study. Geometric parameters for these structures are provided in Table 1, and Table 2 presents their zero-point corrected energies, dipole moments, and rotational constants. Conformer B, a structure in which the azido group resides almost directly over the amine nitrogen lone pair electrons, is the lowest energy structure in the set. As such, it is expected to be the most abundant conformer in a gas-phase DMAZ sample. This finding is considered further in the analysis of the experimentally acquired mid-IR absorption spectrum.

The DMAZ structures are distinguished by differences in their -CH_2-CH_2-N_3 chains, and the labeling of the structures was chosen such that alphabetically adjacent conformers are (nominally) transformed into one another by a dihedral angle rotation about a bond in this chain. Figure 2 provides a mapping of these rotations and their (transition state) barriers. It will be noted that inversion at N1 yields a lower energy pathway between G and H than the dihedral angle rotation upon which the labeling scheme was developed. Also, attempts to locate transition states directly linking B with C and K with L were unsuccessful, but this issue was not pursued once a path capable of linking all equilibrium structures was established. The mapping suggests that there are no significant (kinetic) barriers to an equilibrium distribution of conformer populations forming in a room temperature sample.
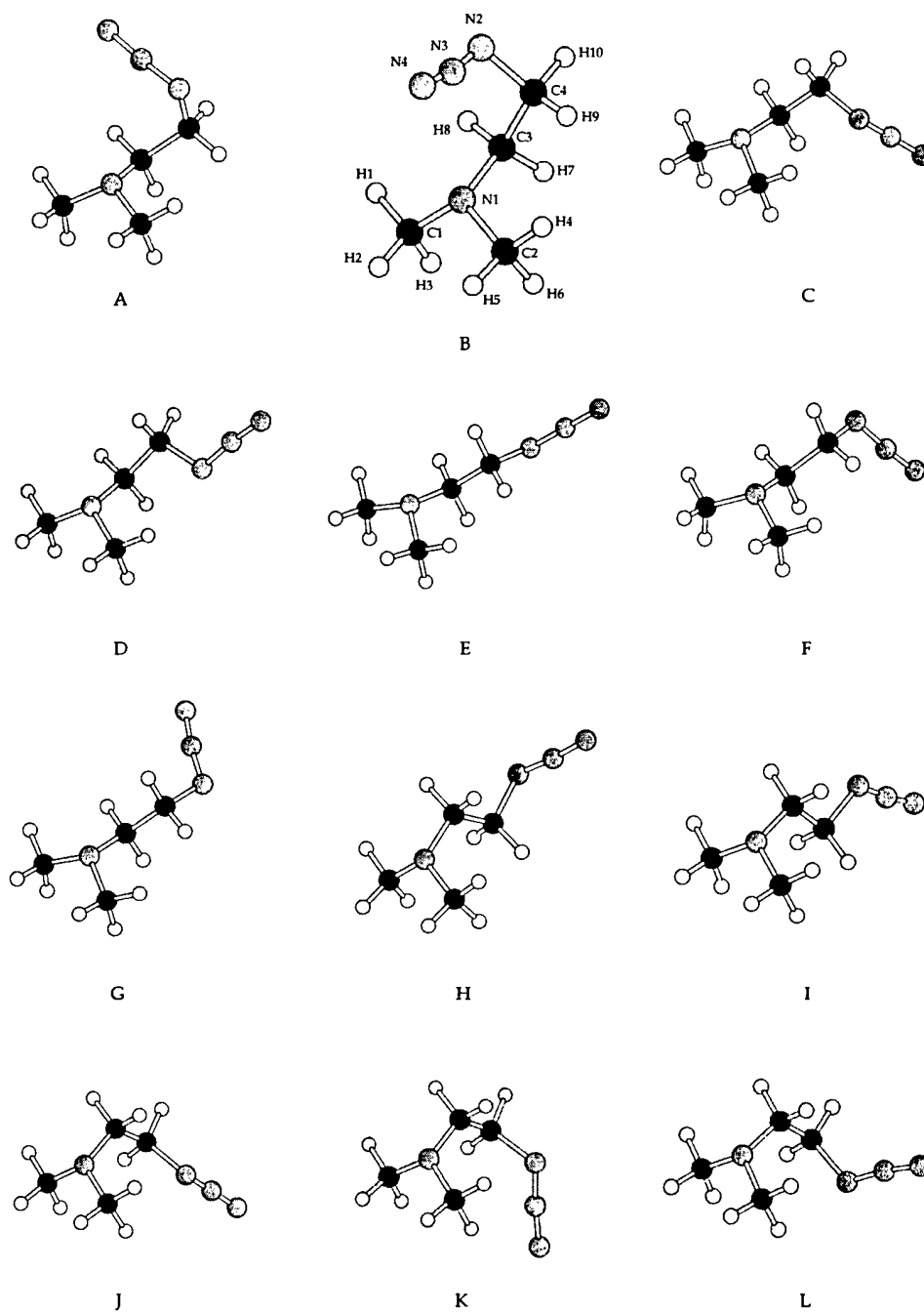
Figure 1. The 12 equilibrium conformers of DMAZ identified via B3LYP/6-311++G(d,p).
Conformer B is the lowest energy structure.

Table 1. Geometric parameters for equilibrium DMAZ conformers obtained via B3LYP/6-311++G(d,p).

Parameter[a]	Conformer											
	A	B	C	D	E	F	G	H	I	J	K	L
Bond Length (in Angstroms)												
C1N1	1.457	1.458	1.459	1.459	1.459	1.459	1.459	1.455	1.455	1.452	1.452	1.454
C2N1	1.457	1.458	1.461	1.462	1.459	1.459	1.459	1.455	1.455	1.458	1.456	1.458
H1C1	1.093	1.092	1.093	1.093	1.092	1.092	1.092	1.093	1.093	1.094	1.094	1.094
H2C1	1.092	1.093	1.092	1.093	1.093	1.093	1.093	1.094	1.094	1.094	1.094	1.093
H3C1	1.106	1.106	1.106	1.106	1.106	1.106	1.106	1.105	1.105	1.105	1.105	1.105
H4C2	1.091	1.092	1.089	1.088	1.091	1.091	1.091	1.093	1.093	1.092	1.092	1.093
H5C2	1.092	1.092	1.092	1.093	1.092	1.092	1.092	1.094	1.094	1.094	1.094	1.094
H6C2	1.107	1.106	1.106	1.106	1.106	1.106	1.106	1.105	1.105	1.101	1.103	1.101
C3N1	1.455	1.459	1.458	1.461	1.460	1.459	1.460	1.455	1.455	1.454	1.453	1.453
H7C3	1.109	1.107	1.108	1.106	1.105	1.107	1.105	1.094	1.094	1.097	1.097	1.097
H8C3	1.095	1.093	1.094	1.094	1.093	1.093	1.094	1.096	1.094	1.094	1.094	1.096
C4C3	1.532	1.531	1.534	1.526	1.527	1.535	1.535	1.546	1.539	1.536	1.544	1.546
H9C4	1.089	1.096	1.096	1.097	1.095	1.089	1.095	1.095	1.096	1.096	1.095	1.090
H10C4	1.097	1.091	1.089	1.095	1.095	1.095	1.089	1.09	1.096	1.098	1.094	1.098
N2C4	1.478	1.476	1.484	1.485	1.482	1.481	1.481	1.481	1.483	1.484	1.483	1.482
N3N2	1.227	1.230	1.228	1.228	1.227	1.229	1.229	1.229	1.228	1.228	1.226	1.228
N4N3	1.136	1.134	1.136	1.136	1.136	1.136	1.136	1.136	1.136	1.136	1.137	1.137
Simple Angle (in Degrees)												
C1N1C2	111.7	111.3	110.9	110.7	110.9	111.0	111.0	113.2	113.1	113.0	113.2	112.9
H1C1N1	109.9	109.9	110.1	110.1	109.9	109.9	110.0	109.7	109.7	109.9	109.9	109.9
H2C1N1	109.6	109.5	109.5	109.4	109.5	109.5	109.5	109.3	109.4	109.4	109.4	109.3
H3C1N1	113.0	113.0	113.0	113.0	113.0	113.0	113.0	114.2	114.2	114.2	114.2	114.1
H4C2N1	110.6	110.8	110.6	110.5	110.8	110.8	110.8	109.7	109.7	109.7	109.8	109.6
H5C2N1	109.3	109.6	109.2	109.2	109.5	109.5	109.5	109.3	109.4	108.9	109.1	109.0
H6C2N1	112.8	112.5	112.4	112.3	112.5	112.6	112.5	114.2	114.2	114.0	114.3	113.9
C3N1C1	111.4	112.6	111.3	111.5	111.9	112.0	112.0	114.9	115.0	114.8	115.2	114.7
H7C3N1	112.3	112.1	112.2	112.3	112.3	111.9	112.3	108.4	108.5	107.5	107.6	107.7
H8C3N1	107.6	108.4	107.3	107.3	108.5	108.5	108.0	108.0	108.5	108.2	108.3	108.1
C4C3N1	114.6	112.8	114.6	114.7	112.0	112.1	111.9	116.5	116.4	118.9	119.1	118.8
H9C4C3	111.5	111.4	109.0	108.7	109.5	109.3	109.7	111.2	110.9	111.0	111.3	110.8
H10C4C3	108.3	109.1	109.3	109.3	111.4	111.7	111.2	110.7	110.9	108.5	108.0	108.7
N2C4C3	115.3	112.7	115.3	111.3	107.6	111.5	111.9	111.4	107.3	110.2	112.5	114.8
N3N2C4	117.0	117.1	116.2	115.9	116.1	116.5	116.4	116.5	116.0	116.0	117.2	116.4
N4N3N2	173.0	171.7	173.3	173.8	173.6	173.0	173.0	173.0	173.8	173.8	173.7	173.3
Dihedral Angle (in Degrees)												
H1C1N1C2	175.6	175.4	175.4	175.2	175.6	175.5	175.5	176.6	176.5	175.0	174.6	175.6
H2C1N1C2	57.1	59.6	56.8	56.7	57.0	57.0	57.0	58.5	58.4	56.9	56.4	57.5
H3C1N1C2	−63.4	−63.5	−63.5	−63.5	−63.3	−63.4	−63.4	−61.9	−61.9	−63.3	−63.7	−62.7
H4C2N1C1	−171.5	−176.4	−175.6	−177.9	−175.7	−175.7	−175.8	−176.7	−176.5	−178.2	−179.7	−177.0
H5C2N1C1	−53.5	−58.0	−56.5	−58.5	−57.2	−57.3	−57.4	−58.6	−58.4	−60.0	−61.4	−59.2
H6C2N1C1	66.7	62.6	63.4	61.5	63.1	63.1	63.0	61.7	61.9	60.9	58.7	61.7
C3N1C1C2	128.0	128.0	127.6	127.3	127.0	127.1	127	135	135.0	136.6	137.8	135.7
H7C3N1C1	−68.0	−82.5	−72.0	−78.9	−79.1	−79.6	−79.2	55.0	55.1	58.7	58.1	58.7
H8C3N1C1	48.7	35.4	44.5	38.2	38.7	38.1	38.5	170.4	170.7	173.9	173.3	173.3
C4C3N1C1	170.0	154.6	162.3	155.7	157.5	156.7	157.5	−67.1	−67.1	−62.2	−62.9	−62.0
H9C4C3N1	67.8	58.1	−157.9	−162.2	−58.1	−58.9	−57.6	−59.6	−60.2	50.0	50.2	50.6
H10C4C3N1	−174.8	176.6	−39.7	−43.7	61.6	60.6	61.9	60.5	60.1	168.2	168.3	168.5
N2C4C3N1	−51.5	−66.7	78.9	78.1	−178.3	−175.8	178.8	177.1	180.0	−72.1	−74.7	68.2
N3N2C4C3	−47.0	80.6	74.9	−177.3	−179.3	−81.3	77.4	78.9	179.7	175.5	113.1	−71.0
N4N3N2C4	−179.7	169.1	176.2	−179.9	−179.8	−174.3	175.3	173.9	−179.9	−179.3	−179.0	−177.4

[a] Refer to Figure 1 for labeling.

Table 2. Relative zero-point corrected energies, dipole moments, and rotational constants of equilibrium DMAZ conformers as computed via B3LYP/6-311++G(d,p).

Conformer Designation	ΔE (kcal/mol)	μ (Debye)	Rotational Constants (GHz)		
A	1.2	3.11	3.30	1.30	1.12
B	—[a]	3.13	3.00	1.38	1.20
C	1.3	2.36	4.46	1.03	0.97
D	1.0	2.53	5.93	0.90	0.82
E	0.4	2.74	7.10	0.76	0.71
F	0.8	2.67	4.93	0.87	0.84
G	0.9	2.78	5.10	0.90	0.79
H	1.9	2.75	5.02	0.92	0.84
I	1.6	2.49	5.73	0.80	0.78
J	2.0	2.01	4.18	1.01	0.96
K	2.4	2.22	3.10	1.34	1.17
L	2.2	2.31	4.10	1.17	1.05

[a] Zero-point corrected energy is –377.325354 hartrees.

The labeling scheme is also predicated on grouping conformers according to one of two predicted (minimum energy) C4C3N1C1 dihedral angles and one of two predicted N2C4C3N1 dihedral angles. As will be discussed, many conformer specific differences in zero-point corrected energy and the frequency and/or transition linestrengths of nominally similar normal modes, correlate with these groups. The groups are therefore an aid in analyzing the experimentally acquired spectrum. Energy and normal mode differences correlating with a third distinguishing geometric parameter—the N3N2C4C3 dihedral angle—are also observed. Unfortunately, a scheme to group conformers according to their N3N2C4C3 dihedral angle was precluded by the priority given to grouping conformers according to C4C3N1C1 and N2C4C3N1 values.

The C4C3N1C1 dihedral angle indicates the orientation of the CH_2 group about the $(CH_3)_2N$-CH_2 bond. Structures A–G have C4C3N1C1 dihedral angles near 160° and are referred to as "trans C4C1" conformers. Structures H–L have C4C3N1C1 dihedral angles near –65° and are referred to as "gauche C4C1" conformers. It is observed that for conformer pairs whose only (primary) difference is their C4C3N1C1 dihedral angle—(A,L), (C,L), (D,J), (E,I), (F,H), and (G,H)—the zero-point corrected energy of the trans C4C1 conformer is about 1 kcal/mol lower than it is in the gauche C4C1 conformer. Conformers B and K are also a pair whose only (primary) difference is their C4C3N1C1 dihedral angle, but the difference in their energies is larger (2.4 kcal/mol). In this case, however, the interaction between the central azido nitrogen atom and the amine lone pair electrons, which is unique to conformer B, presumably contributes to this difference.

6

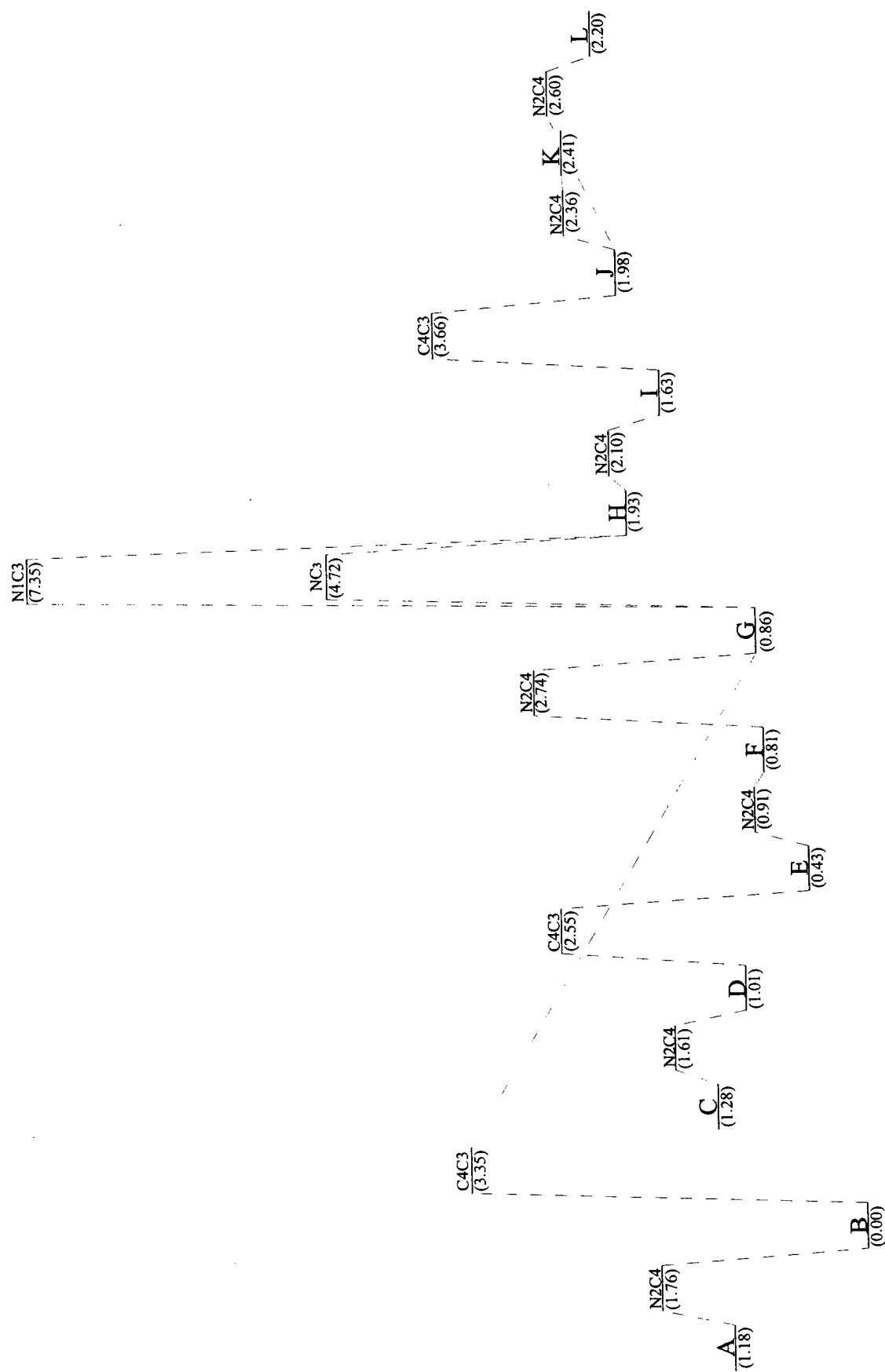Figure 2. A mapping of transition states that connect the 12 identified DMAZ equilibrium structures. For a transition state corresponding to dihedral angle rotation about a bond, the state is labeled with the atoms that define the bond. NC_3 indicates inversion at the amine nitrogen. Structure energies (in kilocalories per mole) relative to the lowest energy structure are shown in parentheses.

The N2C4C3N1 dihedral angle indicates the orientation of the CH_2 groups about the CH_2-CH_2 bond. Structures A–D and J–L have N2C4C3N1 dihedral angles near (±)70°, and are referred to as "*gauche N2N1*" conformers. Structures E–I have N2C4C3N1 dihedral angles near 180° and are referred to as "*trans N2N1*" conformers. It is observed that for conformer pairs where the only (primary) difference is this angle—(A,F), (C,G), (D,E), (J,I), (K,H), and (L,H)—the *trans N2N1* conformer is predicted to be from 0.3 to 0.6 kcal/mol lower in energy. A larger difference (0.9 kcal/mol) is observed in the case of (B,G), but the interaction between the central azido nitrogen and the amine lone pair electrons unique to conformer B is (again) assumed to contribute to this difference.

The N3N2C4C3 dihedral angle indicates the orientation of the azido group relative to the CH_2 group to which it is bonded. Structures D, E, I, and J have N3N2C4C3 dihedral angles near 180° and are referred to as "*anti N3*" conformers. Structures A, B, C, F, G, H, K, and L have N3N2C4C3 dihedral angles closer to (±)80° and are referred to as "*gauche N3*" conformers. It is observed that for conformer pairs where the N3N2C4C3 dihedral angle is the only (primary) geometric difference—(D,C), (E,F), (E,G), (I,H), (J,K), and (J,L)—the *anti N3* conformer is predicted to be from 0.2 to 0.4 kcal/mol lower in energy.

The structures shown in Figure 1 represent 12 of the 14 unique geometries that can be constructed based on combinations of the geometric preferences observed. The other two structures that can be postulated based on these preferences include: (1) a structure similar to conformer A or conformer B, but with an N3N2C4C3 dihedral angle near 180° and (2) a structure similar to conformer C or conformer D, but with an N3N2C4C3 dihedral angle near 80°. Equilibrium conformers with these characteristics were sought through geometry optimizations started with structures similar to those indicated, but searches for the first structure invariably led to conformer A or B, and searches for the second structure led to conformer C or D. In the case of the first structure, it seems likely that repulsion between the lone pair electrons on N1 and N2 makes this configuration unstable. Construction of the second configuration yields a structure in which N2 is in close proximity to H4, and the repulsion between these two sites probably makes this geometry unstable.

With 18 atoms and C_s symmetry, all DMAZ conformers have 48 normal mode vibrations. Frequency values and linestrengths for transitions to all modes of each conformer are provided in Table 3. This information is the basis upon which the experimentally acquired DMAZ spectrum is analyzed. The nature of the motion in modes observed in the experimental spectrum is discussed in the context of the analysis.

Table 3. Normal mode frequencies and transition linestrengths for DMAZ conformers A–L as obtained via B3LYP/6-311++G(d,p).

Mode No.	Conformer											
	A		B		C		D		E		F	
	ν	A	ν	A	ν	A	ν	A	ν	A	ν	A
1	34	0	48	0	39	0	29	0	29	0	36	0
2	51	0	62	0	49	1	52	1	67	4	48	1
3	145	3	99	1	132	2	127	3	105	1	103	1
4	165	1	217	1	211	2	189	2	114	0	191	2
5	238	1	233	0	245	2	236	1	231	1	233	0
6	251	0	251	1	252	2	241	2	235	1	240	4
7	306	3	288	3	282	5	274	3	274	4	262	1
8	340	8	342	7	334	4	309	3	310	1	340	1
9	379	2	407	2	376	4	381	5	386	9	387	13
10	432	1	428	1	430	0	430	0	435	4	427	3
11	541	4	522	7	516	3	512	5	469	1	472	1
12	562	11	557	13	556	12	555	7	549	8	555	8
13	693	18	651	7	656	9	642	16	662	17	675	18
14	782	12	782	23	782	24	781	13	800	1	802	4
15	838	10	849	6	849	7	852	7	854	25	856	12
16	941	20	962	20	946	22	952	30	955	21	927	30
17	987	13	985	17	995	20	1014	17	1046	43	1028	14
18	1060	21	1057	26	1060	22	1059	9	1059	14	1057	25
19	1078	16	1067	3	1069	7	1060	25	1073	3	1065	25
20	1084	12	1073	12	1086	20	1098	16	1090	11	1093	16
21	1118	9	1116	7	1117	5	1116	5	1116	6	1116	7
22	1172	14	1171	13	1173	7	1174	9	1171	10	1177	8
23	1210	10	1206	6	1208	16	1210	25	1198	10	1207	7
24	1275	6	1272	6	1257	3	1253	8	1272	19	1272	14
25	1298	5	1304	16	1301	9	1302	9	1300	11	1298	15
26	1309	12	1315	10	1335	62	1329	158	1326	38	1329	10
27	1336	176	1342	161	1335	118	1346	38	1341	192	1330	113
28	1394	6	1384	7	1382	2	1386	51	1349	2	1363	41
29	1416	8	1405	9	1406	23	1413	6	1421	1	1412	6
30	1443	1	1443	1	1444	1	1444	2	1444	2	1444	1
31	1470	1	1466	0	1469	1	1467	1	1472	0	1471	0
32	1485	7	1485	5	1484	7	1478	18	1485	6	1485	5
33	1488	5	1486	5	1488	4	1485	7	1492	6	1492	5
34	1497	18	1497	3	1488	8	1487	8	1496	15	1498	18
35	1502	12	1500	10	1499	22	1488	14	1501	7	1501	4
36	1511	7	1501	20	1503	11	1502	11	1509	16	1509	13
37	1513	11	1512	11	1515	14	1514	12	1513	9	1513	10
38	2233	530	2236	529	2227	595	2235	707	2237	699	2228	599
39	2876	68	2896	61	2887	51	2907	54	2910	48	2903	40
40	2902	54	2910	48	2907	44	2914	71	2916	88	2911	47
41	2913	189	2920	207	2917	168	2925	154	2929	137	2922	173
42	3012	50	3025	34	3018	29	3002	30	3015	29	3034	21
43	3043	16	3059	24	3051	20	3053	32	3053	18	3058	30
44	3057	29	3065	28	3056	47	3054	19	3057	27	3066	41
45	3069	23	3073	19	3068	32	3061	37	3066	31	3074	15
46	3099	20	3101	10	3098	31	3067	31	3078	29	3100	27
47	3107	28	3103	47	3120	10	3097	33	3100	31	3106	32
48	3117	23	3105	18	3127	11	3134	10	3106	35	3124	15

Notes: ν = cm^{-1}; A = kilometer per mole.

Table 3. Normal mode frequencies and transition linestrengths for DMAZ conformers A–L as obtained via B3LYP/6-311++G(d,p) (continued).

Mode No.	Conformer											
	G		H		I		J		K		L	
	ν	A	ν	A	ν	A	ν	A	ν	A	ν	A
1	37	0	41	0	32	0	31	0	25	0	35	0
2	46	1	50	1	81	4	49	2	42	1	50	1
3	99	0	118	0	111	1	121	3	134	3	140	2
4	193	1	185	0	120	0	194	2	200	1	181	5
5	226	4	231	6	225	1	222	5	241	1	245	1
6	235	1	241	1	246	2	242	1	254	4	250	1
7	261	1	247	0	248	0	253	1	266	4	275	2
8	346	2	322	10	307	5	308	1	303	1	329	3
9	385	11	376	10	382	12	399	4	395	4	399	3
10	429	4	425	0	422	0	435	0	435	0	439	0
11	473	1	486	6	483	5	520	16	517	17	524	11
12	558	9	553	6	550	8	554	8	544	4	558	14
13	677	18	677	16	662	19	631	17	642	15	662	11
14	798	4	786	3	785	1	771	18	754	7	768	10
15	861	25	833	14	831	14	837	3	835	6	828	19
16	927	23	923	18	946	24	926	3	926	5	912	2
17	1028	13	993	7	1034	2	1003	22	974	17	978	14
18	1057	22	1065	53	1061	18	1056	8	1054	13	1053	38
19	1063	31	1067	20	1069	5	1070	8	1072	9	1070	10
20	1093	6	1076	8	1069	50	1080	41	1083	31	1085	29
21	1116	7	1116	10	1117	11	1117	10	1118	11	1117	9
22	1176	12	1173	9	1174	8	1174	7	1173	7	1176	8
23	1208	8	1202	2	1184	2	1194	7	1198	6	1192	4
24	1272	9	1286	10	1290	8	1259	7	1256	9	1266	1
25	1298	15	1313	69	1317	20	1321	25	1325	18	1314	44
26	1308	110	1319	27	1328	149	1332	175	1346	73	1327	79
27	1341	23	1357	62	1339	60	1361	4	1370	56	1365	59
28	1367	46	1370	3	1366	6	1386	38	1384	12	1382	12
29	1417	7	1403	17	1407	2	1397	18	1394	30	1396	27
30	1445	0	1445	0	1444	0	1445	0	1447	0	1445	0
31	1471	0	1465	2	1466	3	1458	2	1457	1	1460	4
32	1485	7	1480	10	1480	9	1477	19	1477	19	1478	10
33	1492	3	1486	6	1487	4	1478	8	1479	8	1480	10
34	1498	13	1493	23	1492	31	1483	7	1484	4	1489	1
35	1502	7	1507	3	1504	3	1494	19	1495	21	1496	19
36	1509	14	1507	6	1507	7	1507	15	1512	7	1510	13
37	1513	9	1522	12	1522	13	1523	11	1527	9	1524	12
38	2229	617	2225	639	2234	680	2234	671	2233	572	2226	595
39	2912	47	2917	47	2913	46	2912	94	2913	82	2921	88
40	2917	79	2923	142	2919	140	2960	89	2940	92	2957	82
41	2929	140	3019	12	3007	28	2995	22	3007	29	2999	8
42	3037	34	3028	47	3031	42	3015	45	3029	41	3012	74
43	3054	7	3046	27	3042	26	3038	38	3041	37	3043	36
44	3058	35	3047	48	3045	13	3041	32	3042	47	3045	37
45	3067	30	3065	20	3046	50	3043	51	3063	20	3046	30
46	3099	21	3089	17	3077	32	3066	31	3078	30	3086	19
47	3106	34	3092	41	3089	25	3084	31	3086	27	3088	43
48	3125	22	3116	21	3091	44	3096	34	3099	27	3116	19

Notes: ν = cm^{-1}; A = kilometer per mole.

10

5. Mid-IR Spectral Analysis

To model the intensity of mid-IR absorption as a function of frequency $[I(v)]$ based on the frequency of the jth normal mode of the ith conformer, vibrational transitions (with rotational line structure contours) were simulated with a Lorentzian lineshape,

$$I(v) = \sum_i \sum_j P(i) A_{i,j} \frac{\gamma / \pi}{\left((b_j v_{i,j} + a_j) - v\right)^2 + \gamma^2},\qquad (1)$$

where $P(i)$ is a (percent of the population) weighting factor for the ith conformer, $A_{i,j}$ is the conformer dependent linestrength for a transition to the jth mode, and γ is the lineshape width at half-maximum. The frequency-scaling factor (b_j) provides an ability to correct for known deficiencies in the scaling of theoretically derived normal mode frequencies [20, 21]. The parameter a_j allows the frequency of the jth mode to be shifted a constant value, its inclusion predicated on accounting for mode anharmonicity.

Prior to summarizing a detailed analysis of the experimentally acquired spectrum, it is instructive to compare it to theoretically based spectral simulations for individual conformers. Shown in Figures 3–5, the simulated spectra in these figures were generated by scaling the normal mode frequencies by the "general" value $(b_{j=1-48} = 0.96)$ recommended by Scott and Radom [21] for B3LYP/6-31G(d) results, setting $a_{j=1-48}$ equal to zero and choosing γ equal to 12 cm^{-1} (based on previous experience in conducting such analyses). The sharp lines between 1400 and 2000 cm^{-1} in the experimentally acquired spectrum are due to water and give an indication of the resolution of the scan. Figure 3 compares the spectra for conformers A, B, C, and D, all of which have *gauche N2N1* and *trans C4C1* dihedral angles. Figure 4 compares the spectra for conformers E, F, and G, all of which have *trans N2N1* and *trans C4C1* dihedral angles. Figure 5 compares the spectra for *gauche C4C1* conformers (H, I, J, K, and L), structures H and I being *trans N2N1* conformers and structures J, K, and L being *gauche N2N1* conformers. It is observed that conformer B's spectrum gives the best (qualitative) agreement with the experimental result, a finding expected based on it being the lowest energy structure. However, B's spectrum alone is not sufficient to explain all of the features observed in the experimentally acquired spectrum. For example, the experimentally observed "triplet" centered at 950 cm^{-1} corresponds to a "doublet" near 920 cm^{-1} in B's spectrum. Similarly, there is a broad shoulder on the experimentally observed feature with a maximum at about 670 cm^{-1}, but B has only a single mode near this frequency.
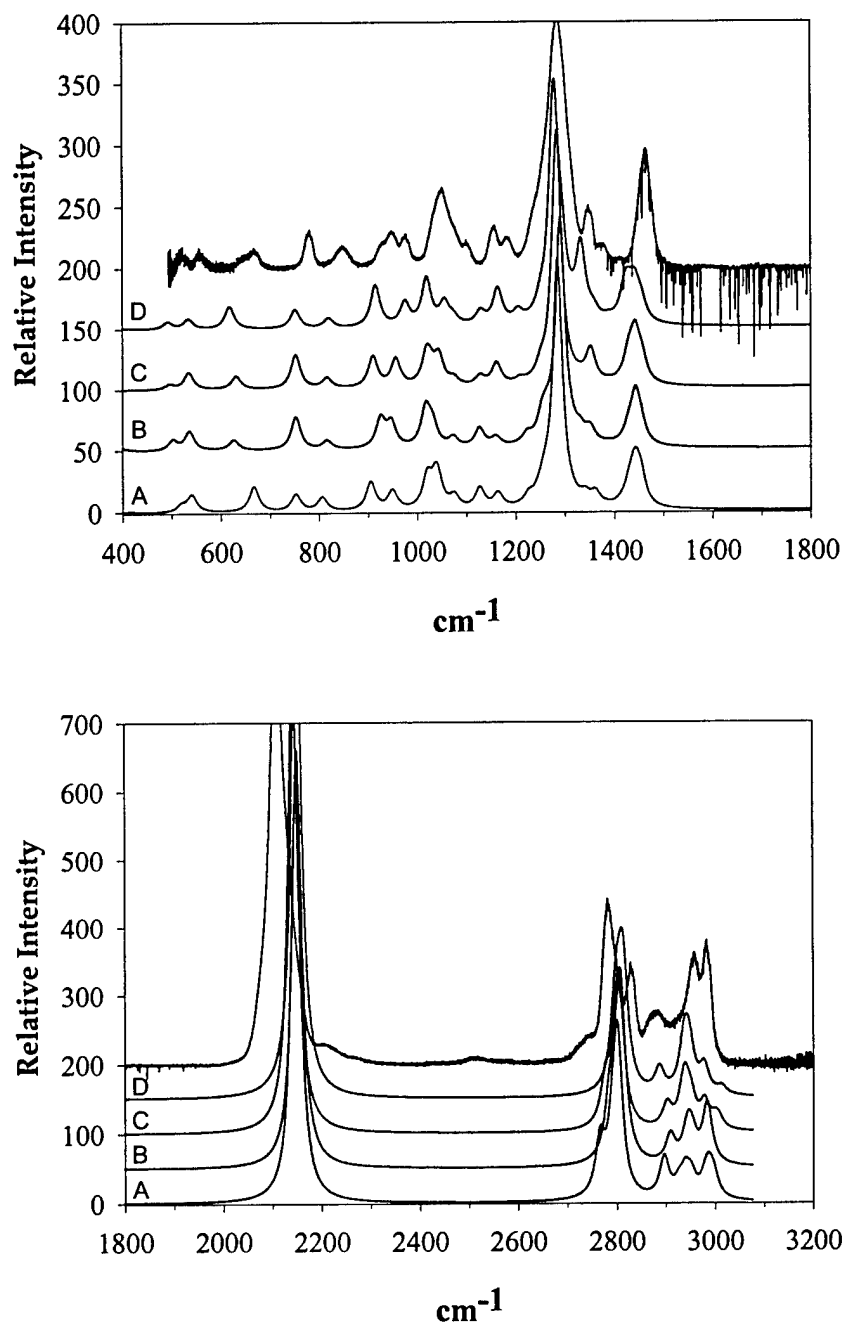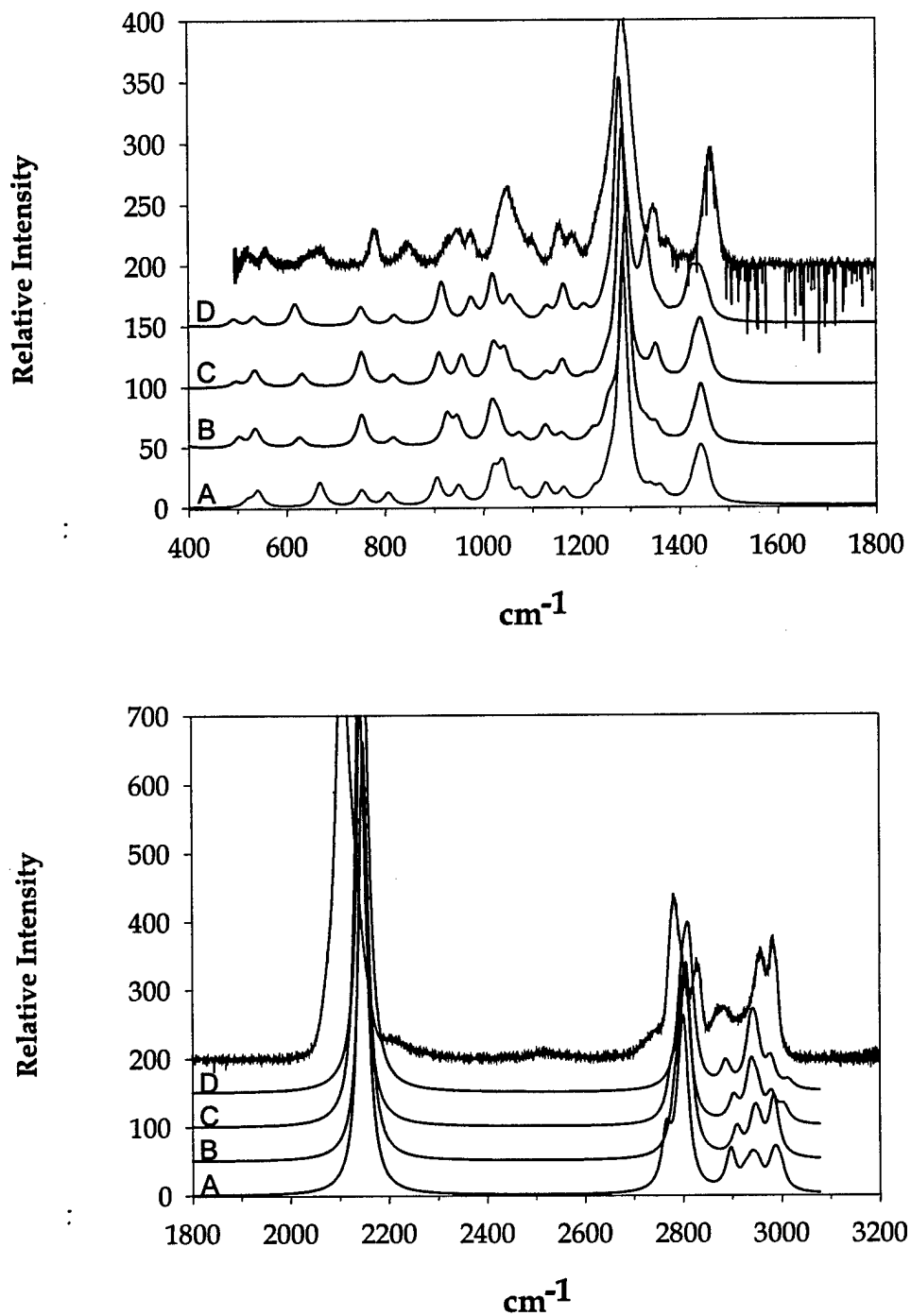
Figure 3. Comparison of the experimentally acquired mid-IR spectrum of DMAZ and simulated spectra for conformers A, B, C, and D, all of which have *trans C4C1* and *gauche N2N1* dihedral angles in their CH_2-CH_2-N_3 chain. The simulations are based on scaling theoretically determined normal mode frequencies by 0.96.

Figure 4. Comparison of the experimentally acquired mid-IR spectrum of DMAZ and simulated spectra for conformers E, F, and G, all of which have *trans C4C1* and *trans N2N1* dihedral angles in their CH_2-CH_2-N_3 chain. The simulations are based on scaling theoretically determined normal mode frequencies by 0.96.
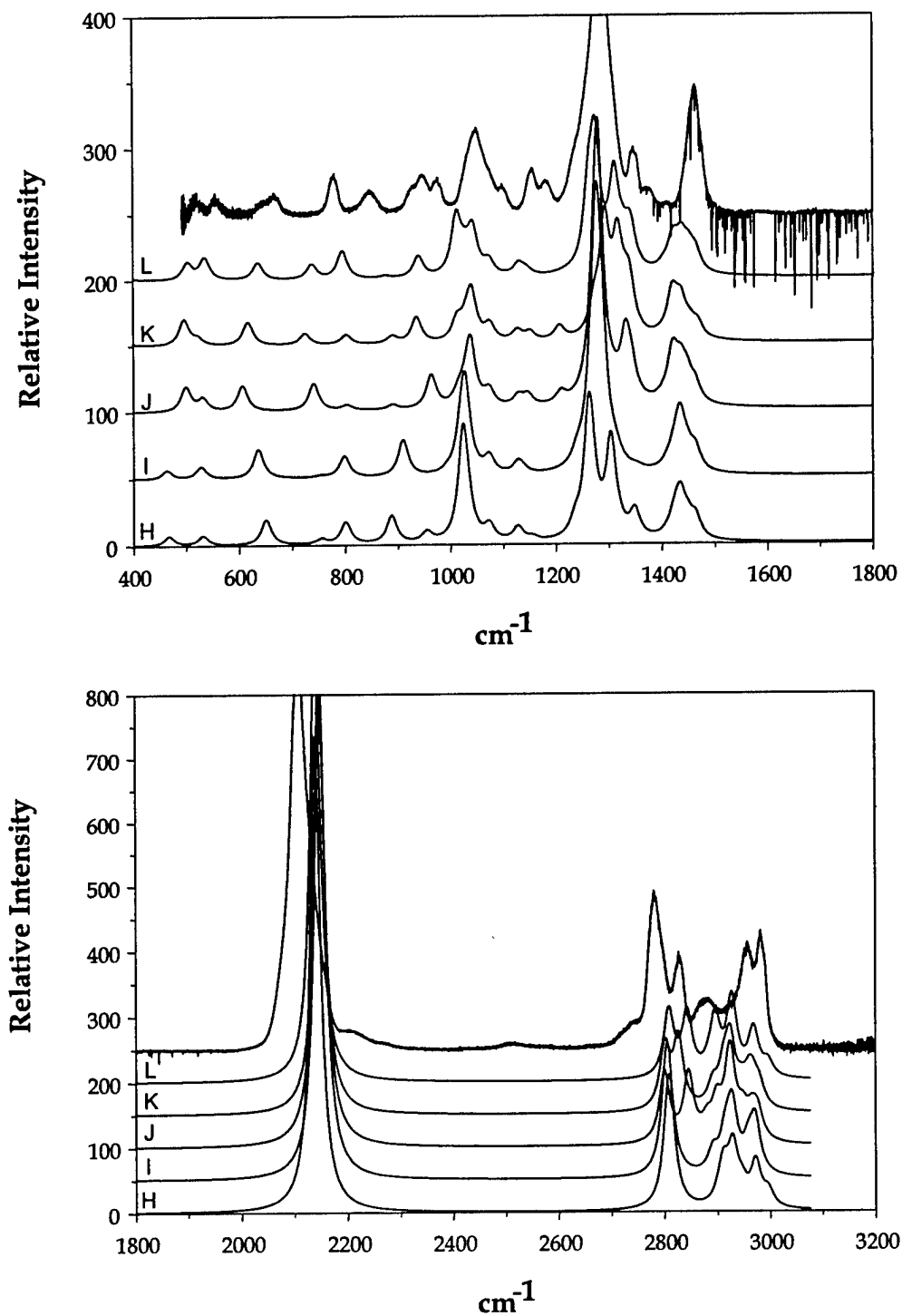
13

Figure 5. Comparison of the experimentally acquired mid-IR spectrum of DMAZ and simulated spectra for conformers H, I, J, K, and L, all of which have a *gauche* C4C1 dihedral angles in their CH_2-CH_2-N_3 chain. The simulations are based on scaling theoretically determined normal mode frequencies by 0.96.

14

Though the "extra" features could be due to vibrational combination bands or an impurity in the sample, it seemed likely (based on their relative energies) that many (if not all) of the theoretically identified DMAZ conformers would be populated in a room temperature sample. Therefore, a non-linear, least-squares fitting routine based on equation 1 was developed to examine this possibility. Initial simulations based on $P(i)$ values corresponding to a Boltzmann distribution calculated from conformer zero-point corrected energies (Table 4) supported the suspicion that conformer B was the lowest energy structure and that other conformers contributed to the spectrum. This motivated the more detailed analysis presented here. However, in conducting the analysis, $P(i)$ values were found to depend strongly on the values of a_j and b_j employed to adjust mode frequencies, and our approach to establishing a_j and b_j values requires comment. First, as shown in Figures 3–5, the "general" scaling factor recommended by Scott and Radom [21] ($b_{j=1-48} = 0.96$) significantly overreduces the frequencies of modes with frequencies in the range of 500–1200 cm⁻¹ ($11 \leq j \leq 23$). Thus their recommendation that b_j be set equal to 1.0013 for "low-frequency" modes appears to be more appropriate for this set. Second, it was found (as expected) that a_j and b_j are strongly interdependent over the small ($\sim$100-cm⁻¹) frequency ranges needed to fit individual spectral features, but that within such ranges, the results produced by the fitting routine are insensitive to specific (a_j, b_j) values when b_j falls within its expected range ($0.96 \leq b_j \leq 1.00$). Based on these findings, and the fact that a_j can be (directly) interpreted/assessed as an anharmonic constant, in all fits to spectral features with frequencies less than 1200 cm⁻¹, b_j was set equal to 1.0, and a_j was the only parameter varied to adjust a mode's frequency.

Table 4. Relative DMAZ conformer populations in a 298-K vapor sample based on theoretically determined zero-point corrected energies.

Conformer Designation	Population Distribution A	Population Distribution B[a]
A	0.053	0.062
B	0.387	0.454
C	0.044	0.051
D	0.070	0.042
E	0.187	0.112
F	0.099	0.116
G	0.091	0.106
H	0.015	0.017
I	0.025	0.015
J	0.014	0.008
K	0.007	0.008
L	0.009	0.011

[a] Empirically corrected distribution obtained following the addition of 0.4 kcal/mol to the zero-point corrected energies of the *anti* N_3 conformers D, E, I, and J.

We also note that beyond the expectation that the shift (and scaling) factors will be mode-dependent, it is possible that they will be conformer-dependent as well—evidence for conformer dependence encountered in the analysis of features associated with modes 13 and 16. It is not certain whether the differences observed are due to (1) real differences in mode anharmonicities for different conformers or (2) computational bias. Regardless, it is assumed that conformer-dependent differences are small compared to mode-dependent differences and that conformer-dependent differences do not change the order (based on magnitude) in which conformer mode frequencies appear.

The mode dependence of a_j effectively precludes a fit of the entire experimentally acquired spectrum prior to analyzing its individual features. In addition, because of the relatively large number of conformers and the similarities in their mode structure, the $P(i)$ are not (typically) independent parameters in the fit of any one feature. Therefore, conformer population weights cannot be determined from fits to individual features alone. However, a characterization of the population distribution emerges from a feature-by-feature analysis of experimentally characterized transitions involving modes 11–17, and these modes are considered in detail. Spectral features associated with transitions to modes 14 and 15 prove to be a good starting point for the analysis, and they are considered first.

5.1 Modes 14 and 15

A strong relationship between the linestrengths for transitions to modes 14 and 15 and a conformer's N2C4C3N1 dihedral angle is observed—high linestrength values for mode 14 being associated with *gauche N2N1* conformers (A, B, C, D, J, K, and L), and high linestrength values for mode 15 being associated with *trans N2N1* conformers (E, F, G, H, and I). This dependence proves to correspond to the fact that mode 14 in *gauche N2N1* conformers and mode 15 in *trans N2N1* conformers involve the same (nominal) normal mode motion, namely, a NC₃ symmetric stretch with a C3-C4-N1 bend. A second observation with ramifications in the analysis is that, within the *trans N2N1* and *gauche N2N1* conformer groups, *gauche C4C1* conformers have lower NC₃ symmetric stretch/C3-C4-N1 bend frequencies than *trans C4C1* conformers.

The experimentally observed features at 780 and 850 cm⁻¹ are associated with transitions to modes 14 and 15, respectively, and, because of the strong frequency and linestrength dependence of these modes on the N2C4C3N1 dihedral angle, their relative intensities reflect the ratio of *trans N2N1* to *gauche N2N1* populations in the vapor. To establish this ratio, the frequency range from 700 to 810 cm⁻¹ was fit first, with all of the parameters in equation 1 (except b_j) treated as variables. Results prove to be sensitive to the parameter values employed to start the fit, with one of two (mutually exclusive) conclusions emerging depending on the starting point. One conclusion is that a_{14} should be

16

approximately -3 cm^{-1} and that the sum of *gauche N2N1/trans C4C1* conformer populations is much greater than the sum of *gauche N2N1/gauche C4C1* conformer populations [$P(A)+P(B)+P(C)+P(D) >> P(J)$, $P(K)$, or $P(L)$]. (Because the theoretically determined frequencies for mode 14 in conformers A, B, C, and D are less than 1 cm^{-1} different, $P(A)$, $P(B)$, $P(C)$, and $P(D)$ are strongly interdependent parameters in the fit of the feature at 780 cm^{-1}, and their values with respect to one another cannot be determined from fits to this feature alone.) The other possible conclusion was that a_{14} should be $+7.5$ cm^{-1} (or greater) and that the population of one of the *gauche N2N1/gauche C4C1* conformers (J, K, or L) is much greater than that of any other conformer, e.g., $P(J) >> P(i)$, $I \neq J$.

In *gauche N2N1/gauche C4C1* conformers (J, K, and L), the frequencies of mode 14 are from 10 to 22 cm^{-1} lower than they are in *gauche N2N1/trans C4C1* conformers (A, B, C, and D). Therefore, simulations with J, K, or L populations that are within about 1 order of magnitude of the sum of A, B, C, and D populations produce two (or more) features near 780 cm^{-1}. Given the one feature observed experimentally, when started with parameter values that lead to an a_{14} value that centers transitions to mode 14 in conformers A, B, C, and D on the band at 780 cm^{-1}, i.e., $a_{14} \approx -3$ cm^{-1}, the fitting routine concludes that the nominal values for $P(J)$, $P(K)$, and $P(L)$ are negligibly small compared to $P(A)+P(B)+P(C)+P(D)$. On the other hand, when started with parameter values that lead to an a_{14} value that centers the transition to mode 14 of conformer J, K, or L on the band at 780 cm^{-1}, the fitting routine concludes that the only conformer with a significant population is the one whose mode 14 frequency is equal to 780 cm^{-1}. For example, in fits with $a_{14} = +7.5$ cm^{-1}, a value that centers the transition to mode 14 of conformer J at 780 cm^{-1}, $P(J)$ is the only $P(i)$ whose nominal value is found to be non-negligible.

Given the theoretically calculated zero-point corrected energies of conformers J, K, and L relative to conformers A, B, C, and D, the expectation is that the sum of the populations of A, B, C and D will be much greater than the populations of J, K or L [$P(A)+P(B)+P(C)$ $P(D) >> P(J)$, $P(K)$, or $P(L)$]. And, despite the alternate possibilities discussed in the preceding paragraph, the case for $P(A)+P(B)+P(C)+P(D) >> P(J)$, $P(K)$, or $P(L)$ is supported by consideration of other results found through the fitting routine. First, an anharmonic contribution to a vibrational mode typically reduces the mode's frequency. The a_{14} value (-3 cm^{-1}) found in fits with $P(A)+P(B)+P(C)+P(D) >> P(J)$ $P(K)$, or $P(L)$ meets this expectation while the a_{14} values ($+7$ cm^{-1}, $+24$ cm^{-1}, or $+10$ cm^{-1}) needed to obtain the results $P(J)$ $P(K)$, or $P(L) >> P(A)+P(B)+P(C)+P(D)$, respectively, do not. Second, many of the other features in the experimentally acquired spectrum (including the feature centered near 850 cm^{-1}) are not well reproduced when $P(J)$, $P(K)$, or $P(L)$ values greater than $P(A)+P(B)+P(C)+P(D)$ are imposed. Thus, the theoretically obtained conclusion that *gauche C4C1* conformers are higher in energy than their *trans C4C1* counterparts appears to be valid, and in the band

analyses that follow, no further consideration is given to population distributions that contradict this conclusion.

Having concluded that a_{14} would have a value near -3 cm^{-1}, the implications of the experimentally observed features at 780 and 850 cm^{-1} were further explored by fitting both at the same time. Limiting a_{14} to values near -3 cm^{-1} and allowing the fitting routine to vary a_{15} and all of the $P(i)$, it was found that, although there was a high statistical uncertainty in individual $P(i)$ values, the nominal values for *gauche N2N1* conformer populations consistently summed to 65%–70% of the total population. This range is slightly higher than the 58% predicted for the sum derived from a Boltzmann distribution of conformer populations based on theoretically determined conformer zero-point corrected energies (Table 4). Figure 6 shows a fit of the bands centered at 780 and 850 cm^{-1} assuming such a distribution, a_{14}, a_{15}, and γ (only) being varied to optimize the fit. Finding a_{14} equal to -3.0 cm^{-1}, a_{15}, equal to -4.7 cm^{-1}, and γ equal to 10 cm^{-1}, except for the fact that the feature at 850 cm^{-1} is slightly too large relative to the one at 780 cm^{-1}, the fit reasonably reproduces the experimentally observed features. (The value for γ is consistent with expectations based on previous experience in conducting such analyses and was fixed to this value in the analysis of all other features.)

Searching to explain why simulated spectra based on the predicted population distribution did not better reproduce the experimental spectrum, the possibility that the discrepancy was related to a systematic underprediction of *anti-N3* conformer (D, E, I, and J) energies was examined. This possibility was suggested by an experimental finding that ethyl azide's *gauche N3* conformer was about 0.1 kcal/mol lower in energy than its *anti N3* conformer (in a nitrogen matrix) [22]. Since the theoretically computed energies of *anti N3* conformers were observed to be from 0.2 to 0.4 kcal/mol lower than otherwise similar *gauche N3* conformers, a conformer population distribution was computed assuming the (relative) energies of *anti N3* conformers were 0.4 kcal/mol higher. The individual conformer population most affected by this adjustment is structure E's—its predicted contribution to the total population falling from 19% to 11% (Table 4). In the adjusted distribution, the *gauche N2N1* conformer populations sum to 64% of the total population. This value is closer to the range indicated by the unconstrained fits to the features at 780 and 850 cm^{-1}, and, as shown in Figure 6, the relative weighting of the experimentally observed features are better reproduced with the adjusted distribution. As will be shown, the adjusted distribution also yields a better fit than the unadjusted one in the case of mode 13, and all other experimentally observed features can be reasonably reproduced with it as well.

The breadth of the feature at 850 cm^{-1} relative to the one at 780 cm^{-1} reflects the fact that mode 15 frequency values for the *trans N2N1* conformers are more varied than mode 14 frequency values for *gauche N2N1* conformers. This led us to examine the possibility of establishing individual $P(i)$ values for *trans N2N1*
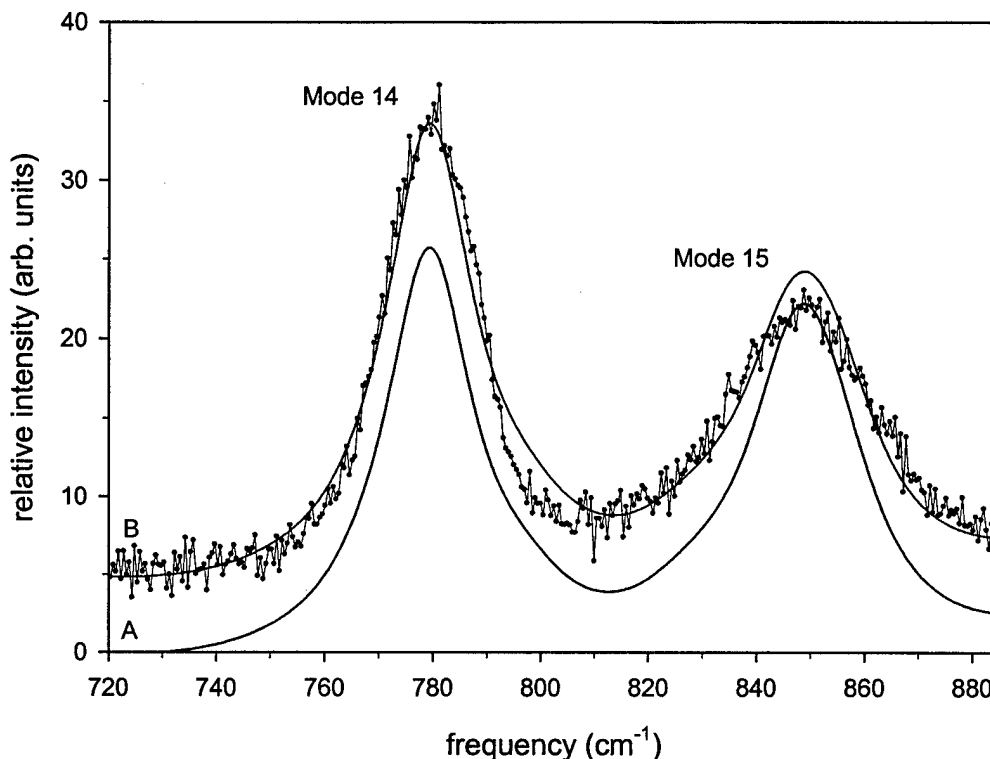
Figure 6. Simulations of transitions to modes 14 and 15 based on the (A) uncorrected and (B) corrected DMAZ conformer populations given in Table 4, a_{14} = -3.0 cm^{-1}, and a_{15} = -4.7 cm^{-1}.

conformers from fits to the feature at 850 cm^{-1}. However, the statistical uncertainty in the $P(i)$ values determined via such fits proved to be large, precluding a meaningful comparison of their values.

5.2 Modes 11 and 12

Mode 11 frequencies for *gauche N2N1* conformers (A–D and J–L) are observed to be significantly higher than mode 11 frequencies for *trans N2N1* conformers (E–I). This difference proves to correlate with the difference in mode 11's motion for the two conformer groups. Mode 11 in *gauche N2N1* conformers involves C1/C2-N1-C3, C3-C4-N1, and C3-N1-N2 bends, the same bends being found in mode 10 of *trans N2N1* conformers. Similarly, mode 10 motion in *gauche N2N1* conformers, which is primarily a C1-N1-C2 bend coupled with N1-C1-C2 and C1-C2-N1 bends, corresponds to mode 11 motion in *trans N2N1* conformers. Thus, the group dependent frequency difference of this bending motion is approximately 90 cm^{-1}.

As for mode 12, in all of the conformers it is an N4-N3-N2 bend with the N3 atom moving perpendicular to the N4-N2-C4 plane. Predicted mode 12 frequencies fall within a fairly narrow range, but two conformational

dependencies are observed. First, the transition linestrengths for this mode are larger in *gauche N2N1* conformers than in *trans N2N1* conformers, a result that is probably due to the N4-N3-N2 bend coupling with a C3-C4-N2 bend in the *gauche-N3* conformers. It is also observed that for five of the six conformer pairs whose only (primary) difference is their N3N2C4C3 dihedral angle—(C,D), (E,F), (E,G), (I,H), and (J,K)—the mode 12 frequency for the *anti N3* conformer is lower. (The exception to this trend is (J,L), but the source of the exception is uncertain.)

The band centered at 520 cm^{-1} in the experimentally acquired spectrum is clearly associated with transitions to mode 11 in *gauche N2N1* conformers, the transitions to modes 10 and 11 in all other conformers being below the low frequency cutoff of the spectroscopic detection system. The lack of experimentally observed transitions below 500 cm^{-1} precludes the comparison between *trans N2N1* and *gauche N2N1* conformer populations that was possible in the analysis of modes 14 and 15, but a fit of the feature at 520 cm^{-1} alone proves to be instructive. First, because the analysis of the features associated with modes 14 and 15 excludes a significant contribution from *gauche N2N1/gauche C4C1* conformers (J, K, and L), the set of possible carriers of the feature at 520 cm^{-1} reduces to just *gauche N2N1/trans C4C1* conformers (A, B, C, or D). Limited to varying the populations of conformers in this set and a_{11}, the fitting routine concludes that only one of these four conformer populations is significant, that population dictated by the value of a_{11}. This behavior follows from the fact that conformers A, B, C, and D have significantly different mode 11 frequencies, and transitions attributable to each would be observed between 500 and 550 cm^{-1} if these conformers existed in comparable concentrations in the sample.

Having reduced the set of possible carriers of the feature at 520 cm^{-1} to conformers A, B, C, or D, consideration of several factors leads to the conclusion that conformer B is the carrier. First, for conformer A to be the primary carrier, an a_{11} value of approximately −19 cm^{-1} has to be imposed to obtain a good fit. In contrast to the a_{11} value (−2 cm^{-1}) found for a population dominated by conformer B, −19 cm^{-1} is much larger than that needed to fit any feature with a frequency less than 1200 cm^{-1}. Also, the 21-cm^{-1} separation between modes 11 and 12 in conformer A is much smaller than the 40-cm^{-1} separation between the two features attributable to these modes in the experimental spectrum. For conformer C or D to be the predominate specie, a_{11} has to be +5 cm^{-1} or +9 cm^{-1}, respectively. Unlike conformer B, which requires the small negative value expected for this parameter, when coupled with the inability of populations dominated by either C or D to adequately reproduce features in the ranges from 900 to 1000 cm^{-1} and 1100 to 1200 cm^{-1}, the results clearly point to conformer B as the lowest energy structure. The rest of the analysis follows from this conclusion.

20

The feature centered near 558 cm⁻¹ is associated with transitions to mode 12, but fits to this feature alone did not yield results that were useful in corroborating the theoretical predictions. However, as shown in Figure 7, fits based on the Table 4 population distributions capably reproduce the features at 520 and 558 cm⁻¹ and are considered further evidence of the validity of the predictions.
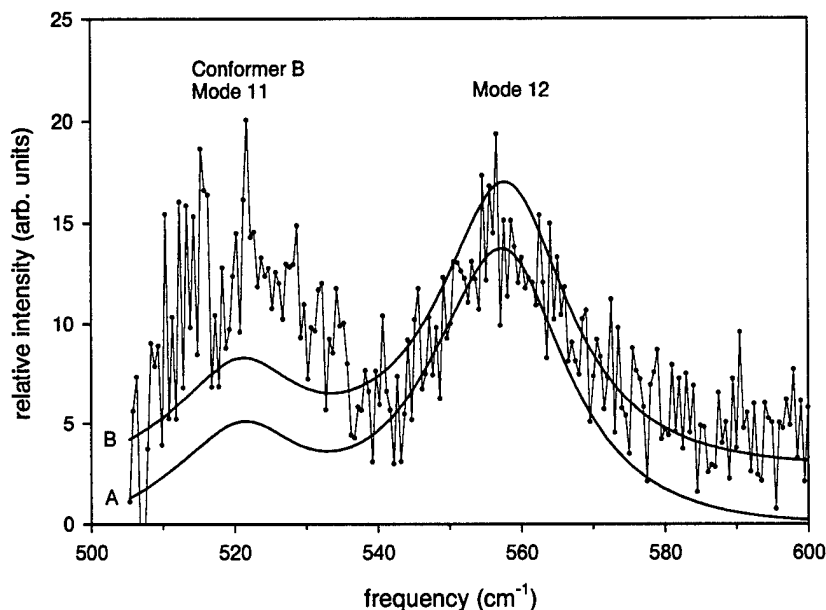

Figure 7. Simulations of transitions to modes 11 and 12 based on the (A) uncorrected and (B) corrected DMAZ conformer populations given in Table 4, $a_{11} = -1.0$ cm⁻¹, and $a_{12} = +1.0$ cm⁻¹.

5.3 Mode 13

In all of the conformers, mode 13 is an N2-N3-N4 bend (that moves in the C4-N2-N4 plane) coupled with a C4-N2-N3 bend. It is found that (with the exception of conformer A) *trans N2N1* conformers have lower mode 13 frequencies than *gauche N2N1* conformers. (The result for conformer A appears to be related to N3's motion aligning with H8 and forcing a significant CH₂ rock.)

In addition, within the *gauche N2N1* and *trans N2N1* conformer groups, *gauche C4C1* conformers have lower mode 13 frequencies than *trans C4C1* conformers. It is also observed that for conformer pairs whose only (primary) difference is their N3N2C4C3 dihedral angle—(E,F), (E,G), (I,H), (J,K) and (J,L)—the mode 13 frequency of the *anti N₃* conformer is lower.

The spectral band centered at 660 cm⁻¹ is associated with transitions to mode 13, and fits to this feature based on the two population distributions in Table 4 are shown in Figure 8. The simulations attribute the low frequency shoulder of the
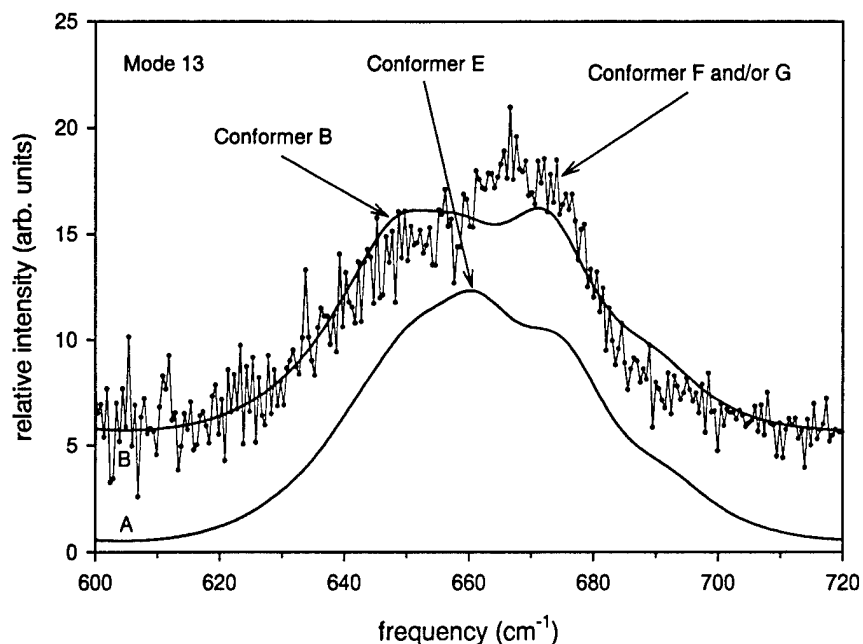
21

Figure 8. Simulations of transitions to mode 13 based on the (A) uncorrected and (B) corrected DMAZ conformer populations given in Table 4, and a_{13} = −3.4 cm⁻¹.

feature to conformer B and the high frequency peak to contributions from *trans N2N1* conformers. In the simulation based on a population distribution derived from (unadjusted) conformer zero-point corrected energies, the main features in the simulation are closer together than in the experimental spectrum. In addition, instead of having the appearance of just two features, the simulation has three distinct features, the central one being attributable to conformer E. Better agreement is observed in the case where the population distribution has been adjusted for the bias suspected in predicted *anti-N₃* energies, the improvement related to the reduced conformer E population in the adjusted distribution.

5.4 Modes 16 and 17

A strong dependence between N2C4C3N1 dihedral angle and the motion of modes 16 and 17 is observed. Mode 16 of *trans N2N1* conformers primarily involves a C4-N2 stretch coupled with C4-N2-N3, C3-C4-N2, and N1-C3-C4 bends. The analogous motion in *gauche N2N1* conformers is observed in mode 17. Mode 16 of *gauche N2N1* conformers is primarily a C1-N1-C2 symmetric stretch coupled with N1-C3-C4 and C3-C4-N2 bends. Not surprisingly, this leads to a relatively large range of values for mode 16 frequencies (923–962 cm⁻¹), but there does not appear to be a correlation between the frequency values or transition linestrengths and the geometric groups considered.

The features associated with transitions to modes 16 and 17 are between 900 and 1000 cm^{-1} in the experimentally acquired spectrum (Figure 9). Given the prior indications that the Table 4 population distributions reasonably reflect reality, the feature with a maximum at approximately 980 cm^{-1} is assignable as the transition to mode 17 in conformer B. It also follows, based on the theoretically calculated difference in frequencies for conformer B modes 16 and 17 (approximately 22 cm^{-1}) that the experimentally observed feature at 950 cm^{-1} is due (in part) to transitions to mode 16 in conformer B. This leaves the low frequency shoulder on the 950 cm^{-1} peak attributable to transitions to mode 16 in *trans N2N1/trans C4C1* conformers. Given the appearance of only one extra feature and the conclusion that the zero-point corrected energies (and populations) of the *trans N2N1* conformers (E, F, and G) are nearly identical, it then follows that the transition to mode 16 in conformer E aligns with the main feature at 950 cm^{-1}, and that conformers F and G are the primary carriers of the low frequency shoulder.
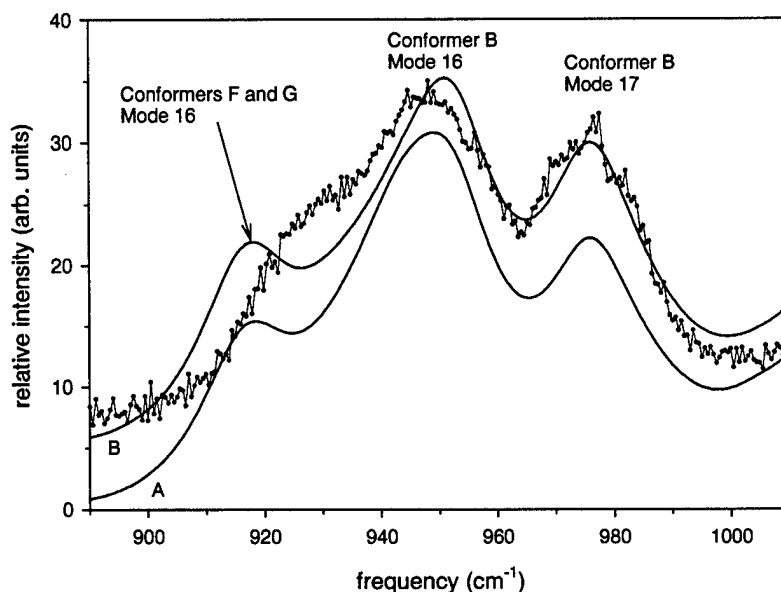

Figure 9. Simulations of transitions to modes 16 and 17 based on the (A) uncorrected and (B) corrected DMAZ conformer populations given in Table 4, a_{16} = −10.2 cm^{-1}, and a_{17} = −8.6 cm^{-1}.

5.5 Modes 18–23

Transitions to modes 18–23 are observed between 1000 and 1200 cm^{-1} in the experimentally acquired spectrum. Shown in Figure 10, simulations of this range based on the two Table 4 population distributions reasonably reproduce the experimental result. The comparison is considered further validation of the theoretical results.
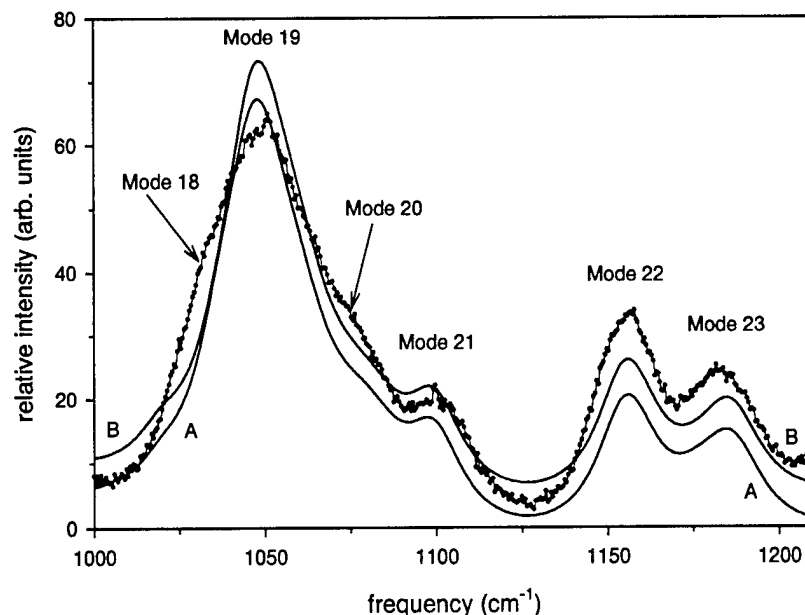
Figure 10. Simulations of transitions to modes 18–23 based on the (A) uncorrected and (B) corrected DMAZ conformer populations given in Table 4, $a_{j=18-20}$ = –11.0 cm^{-1}, $a_{j=21-22}$ = –16.8 cm^{-1}, and a_{23} = –21.6 cm^{-1}.

5.6 Modes 24–37

The spectral features observed in the range from 1200 to 1600 cm^{-1} in the experimentally acquired spectrum are associated with modes 24–37—the strong feature centered at about 1280 cm^{-1} due primarily to a transition to a N2-N3-N4 symmetric stretch, i.e., conformer B mode 27 (Figure 3). Simulations of this range with the two Table 4 population distributions are capable of reasonably reproducing all spectral features. However, because the modes are densely overlapping and the shift/scaling factors are relatively large and mode dependent, there is a higher degree of uncertainty in the assignment of this spectral region than in the others considered.

5.7 Mode 38

In all of the conformers, mode 38 is an antisymmetric N2-N3-N4 stretch, and transitions to this mode produce the strongest feature in the experimentally acquired spectrum, i.e., the one centered at 2100 cm^{-1} (see Figures 3–5). The theoretically determined linestrengths for transitions to this mode are observed to range from about 530 km/mol to almost 700 km/mol, with the three highest values associated with *anti* N$_3$ conformers. However, the frequency values for this mode have little conformer dependence, obviating the usefulness of this feature in characterizing/validating conformer population distributions.

24

5.8 Modes 39–48

Modes 39–48 involve C-H stretches, and transitions to these modes appear between 2700 and 3100 cm⁻¹ in the experimentally acquired spectrum. As is the case for modes 24–37, they are heavily overlapped, limiting our ability to draw conclusions about population distributions based on fits to these features. Simulations of the 2700- through 3100-cm⁻¹ frequency range based on the population distributions given in Table 4 and the (general) frequency scaling factor recommended by Scott and Radom [20] are shown in Figure 11. The simulations are observed to reasonably reproduce the features between 2850 and 3000 cm⁻¹, but not the features between 2700 and 2850 cm⁻¹. In the latter case, instead of three fairly distinct features, only one feature with a low frequency shoulder is produced. We note, however, that all of the conformers have three modes (39, 40, and 41) contributing to this feature. Thus the discrepancy may be due to the fact that a harmonic approximation to the forces does not produce resonance splitting of nearly degenerate C-H stretches. It is also possible that the "extra" feature (or features) is due to a vibrational combination band.
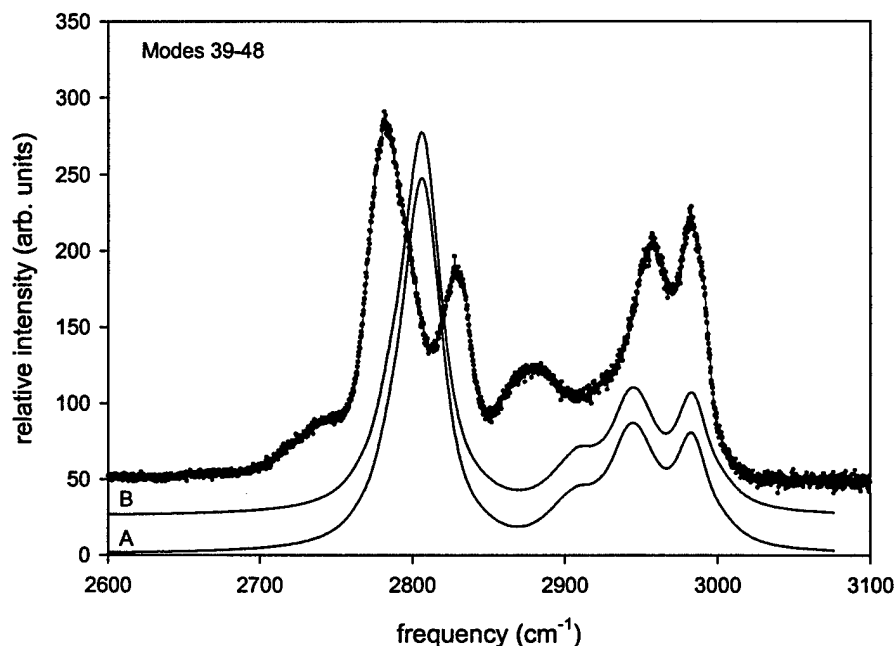

Figure 11. Simulations of transitions to modes 39–48 based on the (A) uncorrected and (B) corrected DMAZ conformer populations given in Table 4. The simulations are based on scaling theoretically determined normal mode frequencies by 0.96.

25

6. Summary

The geometric parameters and normal modes of 12 equilibrium structures of DMAZ have been characterized via non-local DFT. A set of transition states sufficient to connect all identified equilibrium structures was also characterized. Mid-IR absorption spectra of gas-phase DMAZ were obtained experimentally and assigned based on the theoretical results. The spectral analysis indicates that the relative populations of the equilibrium conformers do not deviate significantly from expectations based on a Boltzmann distribution calculated from their zero-point corrected energies. Both the DFT geometry optimizations and the ensuing spectral analysis indicate that the predominant gas-phase conformation is a structure in which the central nitrogen in the azido group aligns over the lone pair electrons of the amine nitrogen. Since this geometry may hinder proton transfer to the amine site, it may be a factor in the fuel's performance as a hypergol.

7. References

1. Frisch, M. J., G. W. Trucks, H. B. Schlegel, G. E. Scuseria, M. A. Robb, J. R. Cheeseman, V. G. Zakrzewski, J. A. Montgomery, R. E. Stratmann, J. C. Burant, S. Dapprich, J. M. Millam, A. D. Daniels, K. N. Kudin, M. C. Strain, O. Farkas, J. Tomasi, V. Barone, M. Cossi, R. Cammi, B. Mennucci, C. Pomelli, C. Adamo, S. Clifford, J. Ochterski, G. A. Petersson, P. Y. Ayala, Q. Cui, K. Morokuma, D. K. Malick, A. D. Rabuck, K. Raghavachari, J. B. Foresman, J. Cioslowski, J. V. Ortiz, B. B. Stefanov, G. Liu, A. Liashenko, P. Piskorz, I. Komaromi, R. Gomperts, R. L. Martin, D. J. Fox, T. Keith, M. A. Al-Laham, C. Y. Peng, A. Nanayakkara, C. Gonzalez, M. Challacombe, P. M. W. Gill, B. G. Johnson, W. Chen, M. W. Wong, J. L. Andres, M. Head-Gordon, E. S. Replogle, and J. A. Pople. Gaussian 98, Revision A.4. Gaussian, Inc., Pittsburgh, PA, 1998.

2. Becke, A. D. "Density-Functional Thermochemistry. 3. The Role of Exact Exchange." *Journal of Chemical Physics*, vol. 98, p. 5648, 1993.

3. Lee, C., W. Yang, and R. G. Parr. "Development of the Colle-Salvetti Correlation-Energy Formula Into a Functional of the Electron-Density." *Physical Review B*, vol. 37, p. 785, 1988.

4. Miehlich, B., A. Savin, H. Stoll, and H. Preuss. "Results Obtained With the Correlation-Energy Density Functionals of Becke and Lee, Yang, and Parr." *Chemical Physics Letters*, vol. 157, p. 200, 1989.

5. Ditchfield, R., W. J. Hehre, and J. A. Pople. "Self-Consistent Molecular-Orbital Methods. 9. Extended Gaussian-Type Basis for Molecular-Orbital Studies of Organic Molecules." *Journal of Chemical Physics*, vol. 54, p. 724, 1971.

6. Hehre, W. J., R. Ditchfield, and J. A. Pople. "Self-Consistent Molecular-Orbital Methods. 12. Further Extensions of Gaussian-Type Basis Sets for Use in Molecular-Orbital Studies of Organic-Molecules." *Journal of Chemical Physics*, vol. 56, p. 2257, 1972.

7. Hariharan, P. C., and J. A. Pople. "Influence of Polarization Functions on Molecular-Orbital Hydrogenation Energies." *Theoretica Chimica Acta*, vol. 28, p. 213, 1973.

8. Hariharan, P. C., and J. A. Pople. "Accuracy of Ah Equilibrium Geometries by Single Determinant Molecular-Orbital Theory." *Molecular Physics*, vol. 27, p. 209, 1974.

9. Gordon, M. S. "The Isomers of Silacyclopropane." *Chemical Physics Letters*, vol. 76, p. 163, 1980.

10. Petersson, G. A., A. Bennett, T. G. Tensfeldt, M. A. Al-Laham, W. A. Shirley, and J. Mantzaris. "A Complete Basis Set Model Chemistry. 1. The Total Energies of Closed-Shell Atoms and Hydrides of the 1st-Row Elements." *Journal of Chemical Physics*, vol. 89, p. 2193, 1988.

11. Clark, T., J. Chandrashakar, G. W. Spitznagel, and P. V. R. Schleyer. "Efficient Diffuse Function-Augmented Basis-Sets for Anion Calculations. 3. The 3-21+G Basis Set for 1st-Row Elements, Li-F." *Journal of Computational Chemistry*, vol. 4, p. 294, 1983.

12. McLean, A. D., and G. S. Chandler. "Contracted Gaussian-Basis Sets for Molecular Calculations. 1. 2nd Row Atoms, Z=11–18." *Journal of Chemical Physics*, vol. 72, p. 5639, 1980.

13. Krishnan, R., J. S. Binkley, R. Seeger, and J. A. Pople. "Self-Consistent Molecular-Orbital Methods. 20. Basis Set for Correlated Wave-Functions." *Journal of Chemical Physics*, vol. 72, p. 650, 1980.

14. Nguyen, M.-T., A. J. Jamka, R. A. Cazar, and F.-M. Tao. "Structure and Stability of the Nitric Acid Ammonia Complex in the Gas Phase and in Water." *Journal of Chemical Physics*, vol. 106, p. 8710, 1997.

15. Tao, F.-M. "Gas Phase Proton Transfer Reaction of Nitric Acid Ammonia and the Role of Water." *Journal of Chemical Physics*, vol. 108, p. 193, 1998.

16. Peng, C., P. Y. Ayala, H. B. Schlegel, and M. J. Frisch. "Using Redundant Internal Coordinates to Optimize Equilibrium Geometries and Transition States." *Journal of Computational Chemistry*, vol. 17, p. 49, 1996.

17. Peng, C., and H. B. Schlegel. "Combining Synchronous Transit and Quasi-Newton Methods to Find Transition-States." *Israel Journal of Chemistry*, vol. 33, p. 449, 1994.

18. Gonzalez, C., and H. B. Schlegel. "An Improved Algorithm for Reaction-Path Following." *Journal of Chemical Physics*, vol. 90, p. 2154, 1989.

19. Gonzalez, C., and H. B. Schlegel. "Reaction-Path Following in Mass-Weighted Internal Coordinates." *Journal of Chemical Physical Chemistry*, vol. 94, p. 5523, 1990.

20. Wong, M. W. "Vibrational Frequency Prediction Using Density Functional Theory." *Chemical Physics Letters*, vol. 256, p. 391, 1996.

21. Scott, A. P., and L. Radom. "Harmonic Vibrational Frequencies: An Evaluation of Hartree-Fock, Moller-Plesset, Quadratic Configuration Interaction, Density Functional Theory, and Semiempirical Scale Factors." *Journal of Physical Chemistry*, vol. 100, p. 16502, 1996.

22. Nielsen, C. J., K. Kosa, H. Priebe, and C. E. Sjogren. "The Vibrational-Spectra, Molecular-Structure and Conformation of Organic Azides. 9. Azidoethane." *Spectrochim*, vol. 44A, p. 409, 1988.

INTENTIONALLY LEFT BLANK.

NO. OF COPIES	ORGANIZATION
2	DEFENSE TECHNICAL INFORMATION CENTER DTIC OCA 8725 JOHN J KINGMAN RD STE 0944 FT BELVOIR VA 22060-6218
1	HQDA DAMO FDT 400 ARMY PENTAGON WASHINGTON DC 20310-0460
1	OSD OUSD(A&T)/ODDR&E(R) DR R J TREW 3800 DEFENSE PENTAGON WASHINGTON DC 20301-3800
1	COMMANDING GENERAL US ARMY MATERIEL CMD AMCRDA TF 5001 EISENHOWER AVE ALEXANDRIA VA 22333-0001
1	INST FOR ADVNCD TCHNLGY THE UNIV OF TEXAS AT AUSTIN 3925 W BRAKER LN STE 400 AUSTIN TX 78759-5316
1	US MILITARY ACADEMY MATH SCI CTR EXCELLENCE MADN MATH THAYER HALL WEST POINT NY 10996-1786
1	DIRECTOR US ARMY RESEARCH LAB AMSRL D DR D SMITH 2800 POWDER MILL RD ADELPHI MD 20783-1197
1	DIRECTOR US ARMY RESEARCH LAB AMSRL CI AI R 2800 POWDER MILL RD ADELPHI MD 20783-1197

NO. OF COPIES	ORGANIZATION
3	DIRECTOR US ARMY RESEARCH LAB AMSRL CI LL 2800 POWDER MILL RD ADELPHI MD 20783-1197
3	DIRECTOR US ARMY RESEARCH LAB AMSRL CI IS T 2800 POWDER MILL RD ADELPHI MD 20783-1197

ABERDEEN PROVING GROUND

NO. OF COPIES	ORGANIZATION
2	DIR USARL AMSRL CI LP (BLDG 305)

ABERDEEN PROVING GROUND

28   DIR USARL
      AMSRL WM BD
        W R ANDERSON
        R A BEYER
        A L BRANT
        S W BUNTE
        C F CHABALOWSKI
        L M CHANG
        T P COFFEE
        J COLBURN
        P J CONROY
        R A FIFER
        B E FORCH
        B E HOMAN
        S L HOWARD
        P J KASTE
        A J KOTLAR
        C LEVERITT
        K L MCNESBY
        M MCQUAID
        M S MILLER
        A W MIZIOLEK
        J B MORRIS
        J A NEWBERRY
        M J NUSCA
        R A PESCE-RODRIGUEZ
        G P REEVES
        B M RICE
        R C SAUSA
        A W WILLIAMS

32

REPORT DOCUMENTATION PAGE

1. AGENCY USE ONLY (Leave blank)	2. REPORT DATE	3. REPORT TYPE AND DATES COVERED
	July 2002	Final, November 1999–January 2002

4. TITLE AND SUBTITLE

Density Functional Theory Characterization of the Structure and Gas-Phase, Mid-Infrared Absorption Spectrum of 2-Azido–N,N-Dimethylethanamine (DMAZ)

5. FUNDING NUMBERS

622618.H80

6. AUTHOR(S)

Michael J. McQuaid, Kevin L. McNesby, Betsy M. Rice, and Cary F. Chabalowski

7. PERFORMING ORGANIZATION NAME(S) AND ADDRESS(ES)

U.S. Army Research Laboratory
ATTN: AMSRL-WM-BD
Aberdeen Proving Ground, MD 21005-5066

8. PERFORMING ORGANIZATION REPORT NUMBER

ARL-TR-2770

9. SPONSORING/MONITORING AGENCY NAMES(S) AND ADDRESS(ES)

10. SPONSORING/MONITORING AGENCY REPORT NUMBER

11. SUPPLEMENTARY NOTES

12a. DISTRIBUTION/AVAILABILITY STATEMENT

Approved for public release; distribution is unlimited.

12b. DISTRIBUTION CODE

13. ABSTRACT (Maximum 200 words)

Non-local density functional theory utilizing the B3LYP exchange-correlation functionals with a 6-311++G(d,p) basis set was employed to characterize the geometric parameters and normal modes of 12 equilibrium conformations of 2-azido–N,N-dimethylethanamine. Also known as DMAZ, an experimentally acquired mid-infrared absorption spectrum of this fuel's vapor is analyzed based on the computational results. The analysis indicates that the relative populations of DMAZ conformers in a room-temperature sample do not deviate significantly from expectations based on a Boltzmann distribution calculated from their theoretically determined zero-point corrected energies. The most abundant conformer is found to have the central nitrogen atom of the azido group aligned over the amine lone pair electrons. Since this configuration is likely to inhibit proton transfer to the amine site, it may play an influential role in DMAZ's performance as a hypergol.

14. SUBJECT TERMS

DMAZ, hypergolic propulsion, DFT, IR absorption, equilibrium geometries

15. NUMBER OF PAGES

39

16. PRICE CODE

17. SECURITY CLASSIFICATION OF REPORT	18. SECURITY CLASSIFICATION OF THIS PAGE	19. SECURITY CLASSIFICATION OF ABSTRACT	20. LIMITATION OF ABSTRACT
UNCLASSIFIED	UNCLASSIFIED	UNCLASSIFIED	UL

INTENTIONALLY LEFT BLANK.